PHOTONICS Research

Mid-infrared chalcogenide microfiber knot resonators

Yu Xie,[1] [iD] Dawei Cai,[1] Hao Wu,[1] Jing Pan,[1] Ning Zhou,[1] Chenguang Xin,[1] Shaoliang Yu,[1] [iD] Pan Wang,[1] [iD] Xiaoshun Jiang,[2] Jianrong Qiu,[1] Xin Guo,[1,*] and Limin Tong[1,3,4]

[1]State Key Laboratory of Modern Optical Instrumentation, College of Optical Science and Engineering, Zhejiang University, Hangzhou 310027, China
[2]National Laboratory of Solid State Microstructures, College of Engineering and Applied Sciences, Nanjing University, Nanjing 210093, China
[3]Collaborative Innovation Center of Extreme Optics, Shanxi University, Taiyuan 030006, China
[4]e-mail: phytong@zju.edu.cn
*Corresponding author: guoxin@zju.edu.cn

A novel type of mid-IR microresonator, the chalcogenide glass (ChG) microfiber knot resonator (MKR), is demonstrated, showing easy fabrication, fiber-compatible features, resonance tunability, and high robustness. ChG microfibers with typical diameters around 3 μm are taper-drawn from As_2S_3 glass fibers and assembled into MKRs in liquid without surface damage. The measured Q factor of a typical 824 μm diameter ChG MKR is about 2.84×10^4 at the wavelength of 4469.14 nm. The free spectral range (FSR) of the MKR can be tuned from 2.0 nm (28.4 GHz) to 9.6 nm (135.9 GHz) by tightening the knot structure in liquid. Benefitting from the high thermal expansion coefficient of As_2S_3 glass, the MKR exhibits a thermal tuning rate of 110 pm · °C^{-1} at the resonance peak. When embedded in polymethyl methacrylate (PMMA) film, a 551 μm diameter MKR retains a Q factor of 1.1×10^4. The ChG MKRs demonstrated here are highly promising for resonator-based optical technologies and applications in the mid-IR spectral range.   © 2020 Chinese Laser Press

https://doi.org/10.1364/PRJ.386395

1. INTRODUCTION

Optical microresonators in the mid-IR spectral region ($\lambda \sim 2.5$–20 μm) are essential components for biochemical sensing, mid-IR spectroscopy, and nonlinear optics [1–3]. To date, mid-IR microresonators have been experimentally realized based on various materials and configurations, such as silicon or chalcogenide glass (ChG) microring resonators [4–8], fluoride crystalline whispering-gallery-mode (WGM) resonators [9–11], semiconductor Fabry–Perot microresonators [12,13], photonic crystal microresonators [14], and Ge-on-Si microresonators [15]. Photonic devices relying on these resonators have shown great potential in a variety of applications, including cavity-enhanced spectroscopy [3,7,8], label-free detection of trace molecules [6], quantum cascade laser (QCL) stabilization [16], and the generation of mid-IR optical frequency combs [5,9,11,15]. However, almost all such resonators are substrate-supported structures that require individual couplers and precise control of the coupling distance, restricting the versatility, flexibility, and fiber compatibility of these mid-IR microresonators in some instances.

In recent years, a novel type of optical microresonator, the microfiber knot resonator (MKR) [17,18], that directly connects to optical fibers via derivative fiber tapers, has emerged with the thriving of microfiber optics [19–23]. By exempting the supporting substrate and the additional coupling structure, as well as offering large fractional evanescent fields and high flexibility, it has attracted increasing attention for use in optical sensors [24,25], lasers [26–28], and many other applications [29]. However, almost all of the reported MKRs (mostly assembled from silica microfibers) are operated in the visible and near-infrared (near-IR) spectral range, and MKRs for mid-IR have not yet been demonstrated.

Owing to their special merits including broadband transparency, high optical nonlinearity, and hospitality to rare-earth dopants, ChGs have been considered as highly promising mid-IR photonic materials [1,30,31]. They have recently been fabricated into optical microcavities in the form of microspheres [32–34], microspheroids [33], microdisks [35,36], microrings [37], bottle-type structures, and microfiber loop resonators (MLRs) [31], although most of them are operated in the near-IR region. At the same time, while ChG microfibers have been successfully fabricated and employed for optical couplers [38], biochemical sensing [39,40], and mid-IR supercontinuum generation [41,42], ChG MKRs for mid-IR have not

been reported so far. Notably, Zhang *et al.* reported a high-Q MKR assembled by a ChG microfiber in the near-IR [43], but this was not extended to the mid-IR region.

Here, we demonstrate ChG MKRs operating in the mid-IR region for the first time, to our knowledge. We fabricate high-quality ChG microfibers by tapering commercial As_2S_3 fibers via a two-step taper-drawing process. In order to avoid surface damage to the microfibers from the mechanical friction that otherwise usually happens due to electrostatic attraction or tensile force of the microfibers in air, we assemble the ChG MKRs in a liquid environment to retain the pristine surface of the as-drawn microfibers, leading to mid-IR MKRs with Q factors typically higher than 10^4 around the 4.5 μm wavelength. Also, we show that, by changing the knot diameter in liquid, the free spectral range (FSR) of the MKR can be precisely tuned from 2.0 nm (28.4 GHz) to 9.6 nm (135.9 GHz). Meanwhile, benefitting from the large thermal expansion coefficient of the As_2S_3 glass (2.14×10^{-5} °C^{-1} [44]), we obtain a thermal tuning rate of 110 pm · °C^{-1} in an 824 μm diameter mid-IR MKR, which is almost 1 order of magnitude larger than that of silica resonators ($\leq$14 pm · °C^{-1} [45]) in the near-IR region. In addition, we show that the free-standing ChG MKR can be readily embedded and integrated onto a solid substrate by solvent polymer while retaining a Q factor above 10^4 around 4.5 μm wavelength.

2. STRUCTURE, FABRICATION, AND CHARACTERIZATION

The ChG microfibers are fabricated with high precision via a two-step taper-drawing process, as shown schematically in Figs. 1(a) and 1(b). Due to the large reduction ratio of fiber diameter between the preform fiber and the final microfiber, here we use the two-step taper-drawing process to ease the tapering system and obtain microfibers with uniform diameters. Similar to that in a typical electrically heated taper-drawing process for silica glass fibers [46], a commercial As_2S_3 fiber (diameter of ~250 μm, core/cladding diameter ratio of 1:20, typical transmission loss of 2.5 dB/m from 4.4 to 4.8 μm, and refractive indices $n_{core} = 2.422$ at 4.6 μm and $n_{clad} = 2.368$ at 4.6 μm) is first heated by an electrical heater (with temperature feedback to control a 6 mm width heating zone) at a temperature slightly higher than the softening temperature of the As_2S_3 glass (~180°C), and stretched bi-directionally at both sides with a speed of 0.4 mm · s^{-1}, until the waist diameter is reduced to around 10 μm [Fig. 1(a)]. Second, the pre-drawn microfiber is stretched unidirectionally at a fast rate of 6 mm · s^{-1} at one end and a slow rate of 0.4 mm · s^{-1} at the other end to draw an uniform-diameter long microfiber with a diameter of about 3 μm [Fig. 1(b)]. The target waist-diameter and waist-length are precisely controllable by setting the
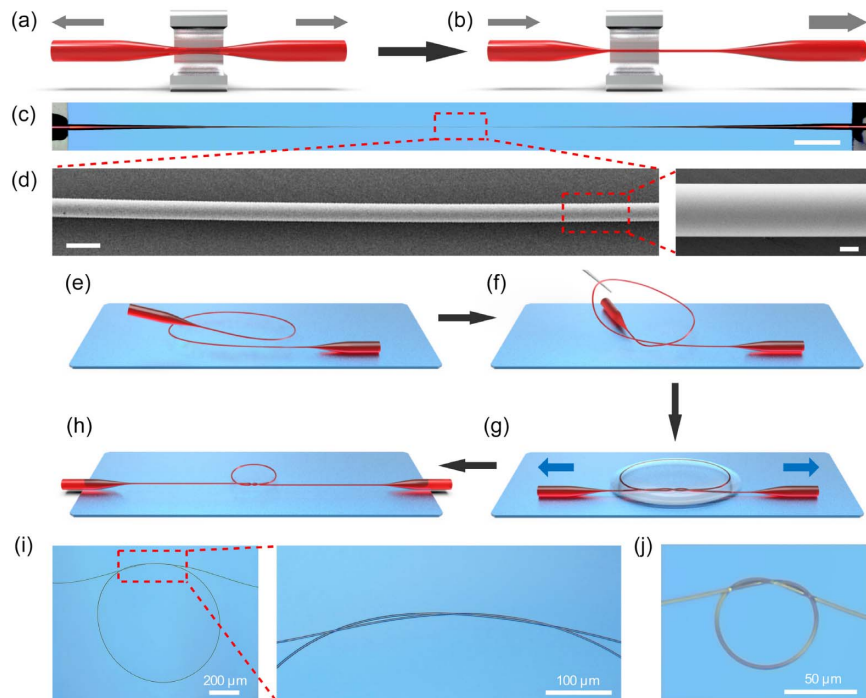

Fig. 1. Fabrications of ChG microfibers and ChG MKRs. (a) and (b) Schematic illustrations of fabrication of a ChG microfiber with controllable waist length and diameter. (c) Optical micrograph of a biconically tapered ChG fiber consisting of a 5.6 μm diameter, 5 mm length ChG microfiber at the central area, and 14 mm length taper area connected to 250 μm diameter initial fiber at both ends. Scale bar, 2 mm. (d) Scanning electron microscope (SEM) image of the microfiber showing the high diameter uniformity. Scale bar, 10 μm. Inset: close-up SEM image of the microfiber, showing excellent sidewall smoothness of the microfiber. Scale bar, 2 μm. (e)–(h) Schematic illustrations of assembly of a ChG MKR in liquid. (i) Optical micrograph of an as-assembled 824 μm diameter ChG MKR using a 3.2 μm diameter ChG microfiber. Inset: close-up optical micrograph of the intertwisted overlap area with an effective coupling length of about 200 μm. (j) Optical micrograph of a 62 μm diameter ChG MKR assembled from a 3.5 μm diameter ChG microfiber.

displacements. Figure 1(c) shows an optical micrograph of an as-drawn 5.6 μm diameter, 5 mm length microfiber within the central area of the biconical waist. Figure 1(d) shows a scanning electron microscope (SEM) image of the microfiber, showing the high diameter uniformity. Additionally, the inset shows a close-up SEM image of the microfiber, indicating excellent sidewall smoothness of the microfiber.

Relying on the micromanipulation under an optical microscope, a biconically tapered long ChG microfiber can be curled up [Fig. 1(e)] and tied into a loose knot [Fig. 1(f)] on a substrate. Made from soft glass, the pristine surface of the ChG microfiber is very likely to be damaged by mechanical friction between fiber areas contacting each other under electrostatic attraction or tensile force of the elastically bent microfiber. To avoid the possible damage, we immerse the microfiber structure in a drop of ethyl alcohol (or deionized water) [Fig. 1(g)] and tighten the knot to the desired size. Finally, when the droplet evaporates, a ChG MKR with good mechanical stability is obtained [Fig. 1(h)]. Figure 1(i) shows optical micrographs of an 824 μm diameter MKR assembled from a 3.2 μm diameter ChG microfiber. In the intertwisted area, the intertwisted overlap length is more than 200 μm [as shown in the inset of Fig. 1(i)], which is long enough for efficient evanescent coupling within the range of 4.45 to 4.8 μm wavelength. In addition, the ChG MKR with minimum diameter obtained is around 62 μm [Fig. 1(j)], which is assembled from a 3.5 μm diameter ChG microfiber, corresponding to a strain of 5.6%. Such a strain is among the highest values reported in ChG fibers [47], indicating the excellent structural uniformity and surface-damage-free condition of the microfiber during the taper drawing and assembling processes.

To investigate the mid-IR response of the ChG MKR, we use a linearly polarized QCL (Daylight Solutions, D11-00028-01) to provide a probing light with a tunable wavelength from 4.45 μm (2247.2 cm^{-1}) to 4.80 μm (2083.3 cm^{-1}). During the measurement, typical optical power coupled into the MKR is ∼1 mW, and an AC-coupled and external liquid-nitrogen-cooled mercury–cadmium–telluride (MCT) photodetector (HORIBA Scientific, DSS-MCT 14-010-E-LN) is used to measure the light output from the MKR. As shown in Fig. 2(a), mid-IR light is coupled into and out of the MKR in free space with ZnSe lenses (Edmund Optics, 88-446). A lock-in amplifier (Stanford Research Systems, SR830) is employed to convert the AC signal output from the detector to DC, and an oscilloscope is employed to extract the signal output from the lock-in amplifier.

Figure 2(b) shows a typical transmission spectrum of a ChG MKR [the same one as shown in Fig. 1(i)] measured with a scanning rate of 5 cm^{-1} · s^{-1}. Broadband resonances are obtained within the whole scanning range, which is mainly attributed to the fundamental modes of the microfiber. The transmission decrease at longer wavelengths is mainly due to the decreases in the wavelength-dependent input power. The FSR is about 3.1 nm (43.9 GHz) around 4.6 μm wavelength [Fig. 2(c)], which agrees well with the perimeter of the MKR (∼2589.6 μm). By Lorentzian fitting of a resonance mode centered at 4469.14 nm wavelength [Fig. 2(d)], we obtain a loaded Q factor of 2.84×10^4, which is comparable with other types of mid-IR
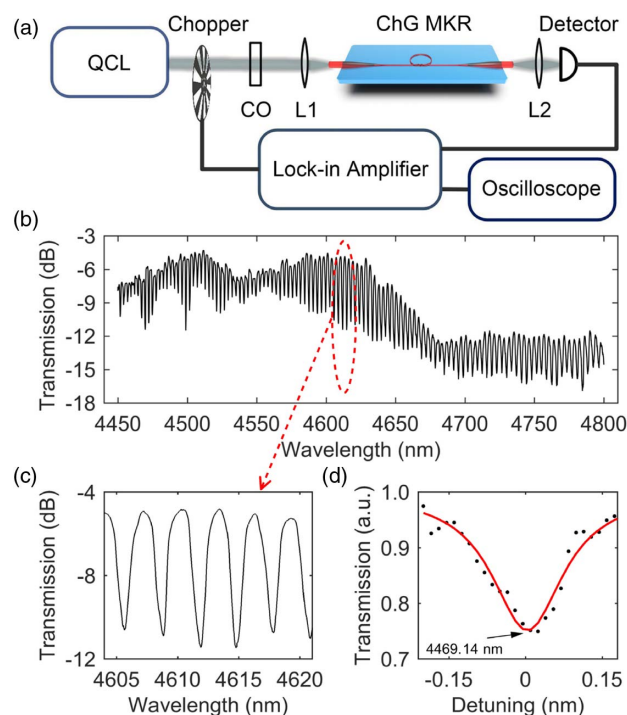

Fig. 2. Mid-IR characterization of a ChG MKR. (a) Schematic illustration of the experimental setup. QCL, quantum cascade laser; CO, free space control optics including polarization controllers (Edmund Optics, 62-770) and homemade silica glass optical attenuators; L1 (L2), ZnSe lens. (b) Typical transmission spectrum of an 824 μm diameter MKR [the one shown in Fig. 1(i)]. (c) Close-up view of the transmission spectrum from 4605 to 4620 nm wavelength, with a measured FSR of about 3.1 nm. (d) Lorentzian fitting (red curve) to a resonance mode (black dots) centered at 4469.14 nm wavelength.

ChG microresonators reported previously [7,35]. Here, the optical loss of the MKR mainly originates from material absorption and scattering leakage, which can be further reduced by using As$_2$S$_3$ fibers with higher material quality, and by preventing contamination during the fabrication and assembly processes.

The knotted structure and its manipulation in liquid also make the MKR quite flexible in fabrication. For example, tightening or loosening the knot can readily change the size, and consequently the FSR of the MKR. Figure 3(a) shows typical transmission spectra of a ChG MKR with diameter decreasing (achieved by tightening the knot in liquid) from 1336 to 749 and 281 μm, resulting in a measured FSR increasing from 2.0 nm (28.4 GHz) to 3.3 nm (46.7 GHz) and 9.6 nm (135.9 GHz), correspondingly. The resonances of the fundamental mode (the dominant dips) of the MKR are maintained well during the tightening process, indicating an opportunity for wide-range tuning of this kind of resonator [48]. The change in the extinction ratio of the resonance modes comes from the change of the intertwisted overlap length and coupling efficiency during the tightening process, and the ripples in the spectrum of the 281 μm diameter MKR come from resonances of higher-order waveguiding modes of the microfiber.
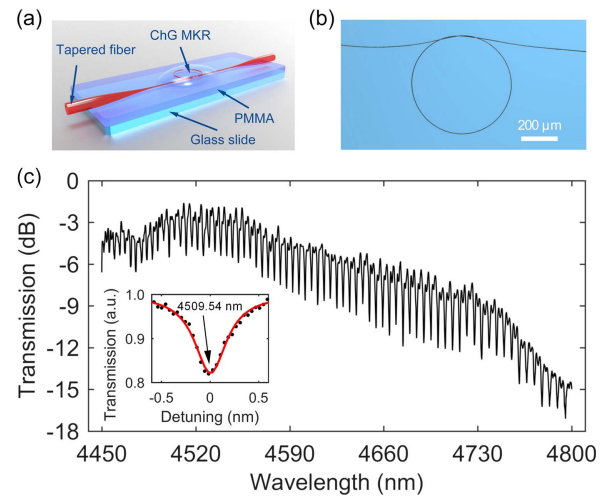
Meanwhile, compared with typical glass materials such as silica glass, As$_2$S$_3$ glass has a much higher thermal expansion
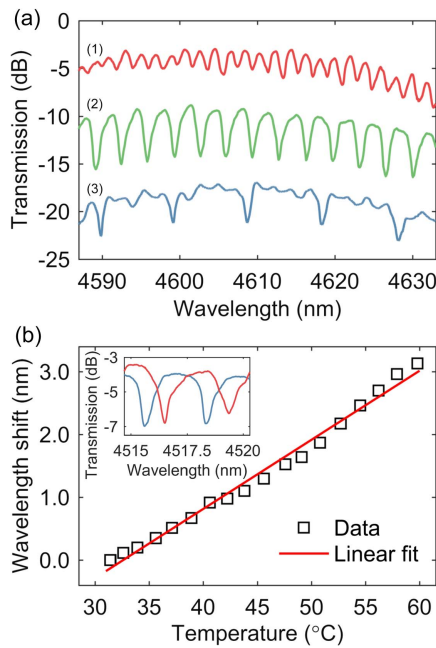
Fig. 3. Spectral tunability of the mid-IR ChG MKRs. (a) Typical transmission spectra of a ChG MKR with diameter decreased successively from (1) 1336 μm to (2) 749 μm and (3) 281 μm by tightening the knot structure in liquid, resulting in the FSR increasing from 2.0 to 3.3 and 9.6 nm, correspondingly. (b) Resonance peak wavelength shift of an 824 μm diameter MKR [the one shown in Fig. 1(i)] with the temperature rising from 31.4°C to 59.8°C, leading to a temperature tuning ratio of 110 pm · °C^{-1} within a spectral range of 3.1 nm. Inset: transmission spectra of resonance modes corresponding to 31.4°C (blue line) and 40.6°C (red line).

Fig. 4. Mid-IR characterization of a PMMA-embedded on-chip ChG MKR. (a) Schematic illustration of a PMMA-embedded on-chip ChG MKR. (b) Optical micrograph of a PMMA-embedded 551 μm diameter ChG MKR assembled from a 3.4 μm diameter microfiber. (c) Transmission spectrum of the embedded MKR shown in (b), with a measured FSR of 4.2 nm and a Q factor of about 1.1×10^4 around 4.5 μm wavelength. Inset: Lorentzian fitting (red curve) to a resonance mode (black dots) centered at 4509.54 nm wavelength.

coefficient $(2.14 \times 10^{-5}$ °C^{-1} of As$_2$S$_3$ glass versus 5.5×10^{-7} °C^{-1} of silica glass), making it much more efficient for thermally tuning the spectral resonance of the MKR. To show this, we control the temperature with an electrical heating plate beneath the ChG MKR, and measure the temperature-dependent resonant response of the MKR. Figure 3(b) shows the temperature-dependent resonant response of the ChG MKR [the same one as shown in Fig. 1(i)], which redshifts from 4518.45 nm to 4521.58 nm with increasing temperature from 31.4°C to 59.8°C, resulting in a tuning range of 3.1 nm. For reference, the inset gives a typical spectrum of resonance shifts from 31.4°C (blue line) to 40.6°C (red line). A thermal tuning rate calculated by linear fitting (110 pm · °C^{-1}, $R^2 \sim 0.994$) is almost 1 order of magnitude higher than that of silica microresonators (≤ 14 pm · °C^{-1}) in the near-IR region. The temperature-dependent resonant response of the ChG MKR mainly originates from the thermal-expansion-induced change of the cavity length [49], and the tuning range and sensitivity of resonance shifts are proved independent of the knot diameter of an MKR in previous work [49].

To show the possibility of on-chip integration of the mid-IR ChG MKR, we embed a free-standing ChG MKR onto a substrate by solvent polymer, as illustrated in Fig. 4(a). The polymer used here is PMMA, which is easy to fabricate, is compatible with ChGs, and has long been used as a fiber coating to protect fragile glass fibers [50]. More importantly, PMMA has

no distinct absorption peak from 4.0 to 5.0 μm wavelength [51], and has a relatively low refractive index (e.g., 1.452 at 4.6 μm [52]). By covering a ChG MKR placed on a substrate with a droplet of PMMA solution prepared by dissolving 3 wt % PMMA in chloroform solution, a PMMA-embedded on-chip MKR can be obtained after the evaporation of chloroform solution within 10 s. Figure 4(b) shows a typical on-chip ChG MKR (551 μm diameter) assembled from a 3.4 μm diameter microfiber. Measured transmission spectrum [Fig. 4(c)] shows that, when embedded in PMMA, the resonant response of the MKR is well maintained, with a loaded Q factor of 1.1×10^4 [inset of Fig. 4(c)] and measured FSR of 4.2 nm (62.2 GHz) around 4.5 μm wavelength. In addition, the on-chip integration isolates the MKR from external contaminations, which significantly increases the long-term stability and offers an opportunity for realizing integrated fiber-compatible high-Q mid-IR resonators for potential applications including molecular sensing [53] and on-chip optical signal processing.

3. CONCLUSION

In conclusion, ChG MKRs have been assembled from taper-drawn ChG microfibers in liquid with high precision and reproducibility. As a novel type of mid-IR microresonator, the ChG MKR shows favorable features including easy fabrication, fiber compatibility, resonance tunability, and high robustness. Typical Q factors of these MKRs are larger than 10^4, and can be further improved by optimizing material and structural parameters. The geometric size and FSR of an individual MKR can be tuned over a wide spectral range, and a large thermal tuning rate of the resonance peak is also observed, which bestows the MKR with high flexibility. Moreover, a free-standing MKR can be readily embedded and integrated onto

a solid substrate while retaining a high-Q factor in the mid-IR, showing the possibility of realizing on-chip, fiber-compatible, high-Q mid-IR microresonators. In addition, the resonator configuration can be extended to passive MKRs fabricated from many other mid-IR optical glasses (e.g., As_2S_3, As-Se-S, and Ge-As-Se), as well as active MKRs with rare-earth dopants. Therefore, the mid-IR MKR demonstrated in this work may find broad applications in the mid-IR region, such as molecular sensing, optical signal processing, lasing technology, and non-linear optics.

Disclosures.   The authors declare no conflicts of interest.

REFERENCES

1. B. J. Eggleton, B. Luther-Davies, and K. Richardson, "Chalcogenide photonics," Nat. Photonics **5**, 141–148 (2011).
2. A. Schliesser, N. Picque, and T. W. Haensch, "Mid-infrared frequency combs," Nat. Photonics **6**, 440–449 (2012).
3. V. Singh, P. T. Lin, N. Patel, H. T. Lin, L. Li, Y. Zou, F. Deng, C. Y. Ni, J. J. Hu, J. Giammarco, A. P. Soliani, B. Zdyrko, I. Luzinov, S. Novak, J. Novak, P. Wachtel, S. Danto, J. D. Musgraves, K. Richardson, L. C. Kimerling, and A. M. Agarwal, "Mid-infrared materials and devices on a Si platform for optical sensing," Sci. Technol. Adv. Mater. **15**, 014603 (2014).
4. R. Shankar, I. Bulu, and M. Lončar, "Integrated high-quality factor silicon-on-sapphire ring resonators for the mid-infrared," Appl. Phys. Lett. **102**, 051108 (2013).
5. A. G. Griffith, R. K. W. Lau, J. Cardenas, Y. Okawachi, A. Mohanty, R. Fain, Y. H. D. Lee, M. J. Yu, C. T. Phare, C. B. Poitras, A. L. Gaeta, and M. Lipson, "Silicon-chip mid-infrared frequency comb generation," Nat. Commun. **6**, 6299 (2015).
6. M. J. Yu, Y. Okawachi, A. G. Griffith, N. Picque, M. Lipson, and A. L. Gaeta, "Silicon-chip-based mid-infrared dual-comb spectroscopy," Nat. Commun. **9**, 1869 (2018).
7. P. Ma, D. Y. Choi, Y. Yu, Z. Y. Yang, K. Vu, T. Nguyen, A. Mitchell, B. Luther-Davies, and S. Madden, "High Q factor chalcogenide ring resonators for cavity-enhanced MIR spectroscopic sensing," Opt. Express **23**, 19969–19979 (2015).
8. Y. Chen, H. T. Lin, J. J. Hu, and M. Li, "Heterogeneously integrated silicon photonics for the mid-infrared and spectroscopic sensing," ACS Nano **8**, 6955–6961 (2014).
9. C. Y. Wang, T. Herr, P. Del'Haye, A. Schliesser, J. Hofer, R. Holzwarth, T. W. Hansch, N. Picque, and T. J. Kippenberg, "Mid-infrared optical frequency combs at 2.5 μm based on crystalline micro-resonators," Nat. Commun. **4**, 1345 (2013).
10. C. Lecaplain, C. Javerzac-Galy, M. L. Gorodetsky, and T. J. Kippenberg, "Mid-infrared ultra-high-Q resonators based on fluoride crystalline materials," Nat. Commun. **7**, 13383 (2016).
11. A. A. Savchenkov, V. S. Ilchenko, F. Di Teodoro, P. M. Belden, W. T. Lotshaw, A. B. Matsko, and L. Maleki, "Generation of Kerr combs centered at 4.5 μm in crystalline microresonators pumped with quantum-cascade lasers," Opt. Lett. **40**, 3468–3471 (2015).
12. T. Schwarzl, W. Heiß, and G. Springholz, "Ultra-high-finesse IV-VI microcavities for the midinfrared," Appl. Phys. Lett. **75**, 1246–1248 (1999).
13. C. G. Xin, H. Wu, Y. Xie, S. L. Yu, N. Zhou, Z. X. Shi, X. Guo, and L. M. Tong, "CdTe microwires as mid-infrared optical waveguides," Opt. Express **26**, 10944–10952 (2018).
14. R. Shankar, R. Leijssen, I. Bulu, and M. Loncar, "Mid-infrared photonic crystal cavities in silicon," Opt. Express **19**, 5579–5586 (2011).
15. Y. H. Guo, J. Wang, Z. H. Han, K. Wada, L. C. Kimerling, A. M. Agarwal, J. Michel, Z. Zheng, G. F. Li, and L. Zhang, "Power-efficient generation of two-octave mid-IR frequency combs in a germanium microresonator," Nanophotonics **7**, 1461–1467 (2018).
16. M. Siciliani de Cumis, S. Borri, G. Insero, I. Galli, A. Savchenkov, D. Eliyahu, V. Ilchenko, N. Akikusa, A. Matsko, L. Maleki, and P. De Natale, "Microcavity-stabilized quantum cascade laser," Laser Photon. Rev. **10**, 153–157 (2016).
17. L. M. Tong, R. R. Gattass, J. B. Ashcom, S. L. He, J. Y. Lou, M. Y. Shen, I. Maxwell, and E. Mazur, "Subwavelength-diameter silica wires for low-loss optical wave guiding," Nature **426**, 816–819 (2003).
18. X. S. Jiang, L. M. Tong, G. Vienne, X. Guo, A. Tsao, Q. Yang, and D. R. Yang, "Demonstration of optical microfiber knot resonators," Appl. Phys. Lett. **88**, 223501 (2006).
19. R. Ismaeel, T. Lee, M. Ding, M. Belal, and G. Brambilla, "Optical microfiber passive components," Laser Photon. Rev. **7**, 350–384 (2013).
20. X. Q. Wu and L. M. Tong, "Optical microfibers and nanofibers," Nanophotonics **2**, 407–428 (2013).
21. L. M. Tong, "Micro/nanofibre optical sensors: challenges and prospects," Sensors **18**, 903 (2018).
22. L. M. Tong, J. Y. Lou, and E. Mazur, "Single-mode guiding properties of subwavelength-diameter silica and silicon wire waveguides," Opt. Express **12**, 1025–1035 (2004).
23. Y. Yu, T. H. Xiao, H. L. Guo, and Z. Y. Li, "Sensing of microparticles based on a broadband ultrasmall microcavity in a freely suspended microfiber," Photon. Res. **5**, 143–150 (2017).
24. X. L. Li and H. Ding, "All-fiber magnetic-field sensor based on micro-fiber knot resonator and magnetic fluid," Opt. Lett. **37**, 5187–5189 (2012).
25. Z. L. Xu, Q. Z. Sun, B. R. Li, Y. Y. Luo, W. G. Lu, D. M. Liu, P. P. Shum, and L. Zhang, "Highly sensitive refractive index sensor based on cascaded microfiber knots with Vernier effect," Opt. Express **23**, 6662–6672 (2015).
26. X. S. Jiang, Q. Yang, G. Vienne, Y. H. Li, L. M. Tong, J. J. Zhang, and L. L. Hu, "Demonstration of microfiber knot laser," Appl. Phys. Lett. **89**, 143513 (2006).
27. X. S. Jiang, Q. H. Song, L. Xu, J. Fu, and L. M. Tong, "Microfiber knot dye laser based on the evanescent-wave-coupled gain," Appl. Phys. Lett. **90**, 233501 (2007).
28. M. Liu, R. Tang, A. P. Luo, W. C. Xu, and Z. C. Luo, "Graphene-decorated microfiber knot as a broadband resonator for ultrahigh repetition-rate pulse fiber lasers," Photon. Res. **6**, C1–C7 (2018).
29. X. S. Jiang, Y. Chen, G. Vienne, and L. M. Tong, "All-fiber add–drop filters based on microfiber knot resonators," Opt. Lett. **32**, 1710–1712 (2007).
30. A. Zakery and S. R. Elliott, "Optical properties and applications of chalcogenide glasses: a review," J. Non-Cryst. Solids **330**, 1–12 (2003).
31. S. Gao and X. Y. Bao, "Chalcogenide taper and its nonlinear effects and sensing applications," iScience **23**, 100802 (2020).
32. F. Vanier, Y. A. Peter, and M. Rochette, "Cascaded Raman lasing in packaged high quality As_2S_3 microspheres," Opt. Express **22**, 28731–28739 (2014).
33. O. Aktas, E. Ozgur, O. Tobail, M. Kanik, E. Huseyinoglu, and M. Bayindir, "A new route for fabricating on-chip chalcogenide microcavity resonator arrays," Adv. Opt. Mater. **2**, 618–625 (2014).
34. O. Aktas, "Chalcogenide microresonators tailored to distinct morphologies by the shaping of glasses on silica tapers," Opt. Lett. **42**, 907–910 (2017).
35. H. T. Lin, L. Li, Y. Zou, S. Danto, J. D. Musgraves, K. Richardson, S. Kozacik, M. Murakowski, D. Prather, P. T. Lin, V. Singh, A. Agarwal, L. C. Kimerling, and J. J. Hu, "Demonstration of high-Q mid-infrared chalcogenide glass-on-silicon resonators," Opt. Lett. **38**, 1470–1472 (2013).
36. N. Singh, D. D. Hudson, R. Wang, E. C. Magi, D. Y. Choi, C. Grillet, B. Luther-Davies, S. Madden, and B. J. Eggleton, "Positive and negative phototunability of chalcogenide (AMTIR-1) microdisk resonator," Opt. Express **23**, 8681–8686 (2015).
37. S. Levy, M. Klebanov, and A. Zadok, "High-Q ring resonators directly written in As_2S_3 chalcogenide glass films," Photon. Res. **3**, 63 (2015).

38. O. Aktas and M. Bayindir, "Tapered nanoscale chalcogenide fibers directly drawn from bulk glasses as optical couplers for high-index resonators," Appl. Opt. **56**, 385–390 (2017).

39. S. Hocde, C. Boussard-Pledel, G. Fonteneau, D. Lecoq, H. L. Ma, and J. Lucas, "Recent developments in chemical sensing using infrared glass fibers," J. Non-Cryst. Solids **274**, 17–22 (2000).

40. J. Keirsse, C. Boussard-Pledel, O. Loreal, O. Sire, B. Bureau, P. Leroyer, B. Turlin, and J. Lucas, "IR optical fiber sensor for biomedical applications," Vib. Spectrosc. **32**, 23–32 (2003).

41. D.-I. Yeom, E. C. Maegi, M. R. E. Lamont, M. A. F. Roelens, L. B. Fu, and B. J. Eggleton, "Low-threshold supercontinuum generation in highly nonlinear chalcogenide nanowires," Opt. Lett. **33**, 660–662 (2008).

42. C. W. Rudy, A. Marandi, K. L. Vodopyanov, and R. L. Byer, "Octave-spanning supercontinuum generation in in situ tapered As$_2$S$_3$ fiber pumped by a thulium-doped fiber laser," Opt. Lett. **38**, 2865–2868 (2013).

43. Q. M. Zhang, M. Li, Q. A. Hao, D. H. Deng, H. Zhou, H. P. Zeng, L. Zhan, X. A. Wu, L. Y. Liu, and L. Xu, "Fabrication and characterization of on-chip optical nonlinear chalcogenide nanofiber devices," Opt. Lett. **35**, 3829–3831 (2010).

44. M. J. Weber, *Handbook of Optical Materials*, 1st ed. (CRC Press, 2003).

45. S. T. Chu, W. Pan, S. Suzuki, B. E. Little, S. Sato, and T. Kokuban, "Temperature insensitive vertically coupled microring resonator add/drop filters by means of a polymer overlay," IEEE Photon. Technol. Lett. **11**, 1138–1140 (1999).

46. J. M. Ward, D. G. O'Shea, B. J. Shortt, M. J. Morrissey, K. Deasy, and S. G. N. Chormaic, "Heat-and-pull rig for fiber taper fabrication," Rev. Sci. Instrum. **77**, 083105 (2006).

47. E. M. Dianov, V. M. Krasteva, V. G. Plotnichenko, S. K. Semenov, M. F. Churbanov, and I. Scripachev, "Mechanical properties of chalcogenide glass optical fibers," Proc. SPIE **0683**, 92–100 (1990).

48. J. Wang, T. R. Zhan, G. S. Huang, P. K. Chu, and Y. F. Mei, "Optical microcavities with tubular geometry: properties and applications," Laser Photon. Rev. **8**, 521–547 (2014).

49. Y. Chen, F. Xu, and Y. Q. Lu, "Teflon-coated microfiber resonator with weak temperature dependence," Opt. Express **19**, 22923–22928 (2011).

50. C. Baker and M. Rochette, "Highly nonlinear hybrid AsSe-PMMA microtapers," Opt. Express **18**, 12391–12398 (2010).

51. S. Sain, D. Ray, A. Mukhopadhyay, S. Sengupta, T. Kar, C. J. Ennis, and P. K. S. M. Rahman, "Synthesis and characterization of PMMA-cellulose nanocomposites by *in situ* polymerization technique," J. Appl. Polym. Sci. **126**, E127–E134 (2012).

52. S. Tsuda, S. Yamaguchi, Y. Kanamori, and H. Yugami, "Spectral and angular shaping of infrared radiation in a polymer resonator with molecular vibrational modes," Opt. Express **26**, 6899–6915 (2018).

53. P. T. Lin, J. Giammarco, N. Borodinov, M. Savchak, V. Singh, L. C. Kimerling, D. T. Tan, K. A. Richardson, I. Luzinov, and A. Agarwal, "Label-free water sensors using hybrid polymer-dielectric mid-infrared optical waveguides," ACS Appl. Mater. Interfaces **7**, 11189–11194 (2015).